

Sampling methods for low-frequency electromagnetic imaging

Bastian Gebauer[†], Martin Hanke[‡] and Christoph Schneider[‡]

[†] RICAM, Austrian Academy of Sciences, Altenbergerstr. 69, 4040 Linz, Austria

[‡] Institut für Mathematik, Johannes Gutenberg-Universität, 55099 Mainz, Germany

E-mail: bastian.gebauer@ricam.oeaw.ac.at, hanke@math.uni-mainz.de and cs@math.uni-mainz.de

Abstract. For the detection of hidden objects by low-frequency electromagnetic imaging the Linear Sampling Method works remarkably well despite the fact that the rigorous mathematical justification is still incomplete. In this work, we give an explanation for this good performance by showing that in the low-frequency limit the measurement operator fulfills the assumptions for the fully justified variant of the Linear Sampling Method, the so-called Factorization Method. We also show how the method has to be modified in the physically relevant case of electromagnetic imaging with divergence-free currents. We present numerical results to illustrate our findings, and to show that similar performance can be expected for the case of conducting objects and layered backgrounds.

Published in: *Inverse Problems* **24** (2008) 015007 (18pp)

Online at: <http://stacks.iop.org/0266-5611/24/015007>

©2008 IOP Publishing Ltd

1. Introduction

For the detection of buried landmines the most frequently used devices are standard *off-the-shelf* metal detectors. These detectors generate (and measure) an electromagnetic field which changes in the vicinity of metallic or magnetic objects. Such a change then triggers (on a more or less heuristic basis) an acoustic signal to indicate that there might be a buried landmine underneath. To improve the reliability of these devices, however, it is necessary to extract more information about the shape and position of magnetic, dielectric or conducting inhomogeneities out of the signal.

Standard metal detectors work with very low frequencies around 20kHz, which corresponds to a wavelength of approximately 15km, while the typical objects of interest are only a few centimeters in size. The problem can therefore be expected to be severely ill-posed, much like electrical impedance tomography (EIT), which can also be considered as a problem of detecting inhomogeneities using waves of infinite wavelength; cf., e.g., Lassas [28] or Cheney, Isaacson and Newell [9]. Because of this, we investigate new non-iterative methods that have recently been used with some success in EIT, but also in inverse scattering, namely the Linear Sampling Method and the Factorization Method.

The Linear Sampling Method was developed under the name *simple method* by Colton and Kirsch in [11]. In this seminal work it was used to detect a scatterer from far field measurements for the Helmholtz equation, and it has since then been applied to a variety of different problems. As a starting point for the interested reader we refer to the recent review article [12] by Colton and Kress, and the many references therein. The method requires measurements for a range of excitations, or to put it in another way, it uses the (typically linear) measurement operator, called M_s^ω below, as given data. A somewhat unusual but useful way of formulating the method is based on a factorization of this operator into a product of two operators

$$M_s^\omega = LG, \tag{1.1}$$

where the range of the operator L (the set of so-called *virtual measurements*) uniquely determines the shape and the position of the scatterer Ω . An immediate consequence of (1.1) is the *range inclusion* $\mathcal{R}(M_s^\omega) \subseteq \mathcal{R}(L)$, from which one can then deduce that a (possibly empty) subset of Ω can be located from the measurements M_s^ω .

For the same problem as in [11] Kirsch developed in [22] a variant of the Linear Sampling Method, for which he could rigorously prove that it reconstructs Ω , and not only a subset. This so-called Factorization Method makes use of a factorization of M_s^ω into L , its adjoint L^* , and a third operator, to show a *range identity* of the form

$$\mathcal{R}(L) = \mathcal{R}(|M_s^\omega|^{1/2}), \tag{1.2}$$

so that $\mathcal{R}(L)$ and thus Ω can be determined from the measurements M_s^ω . The Factorization Method was generalized to applications in EIT by Brühl and Hanke in [5, 6, 20] and in electrostatics by Hähner in [21]. It was successfully applied to several other situations, from which we like to point out two that have immediate relations to

this work, namely harmonic vector fields by Kress in [26, 27] and far-field electromagnetic measurements by Kirsch in [23]. Further applications, and a framework for general real elliptic equations, that we shall utilize later on, can be found in [15].

For the problem of near-field electromagnetic measurements that we consider here, a range identity like (1.2) does not appear to be in reach. In [24], Kirsch proposes to overcome this difficulty by using the measurements to simulate incoming fields. However, according to the numerical results in [18], the original Linear Sampling Method also seems to detect the scatterer, and not only a subset, in this particular setting. In this work we try to give an explanation for this good performance by showing that in the low-frequency limit the measurements are essentially electrostatic measurements, for which the Factorization Method can be shown to work, at least for excitations with non-vanishing divergence as they have been used in [18]. Although this analysis explains the success of the Linear Sampling Method to some extent, it also reveals that the method will fail in the practically relevant case of divergence-free currents, where no electrostatic effects are present. We therefore study the low-frequency asymptotics also for this case, and derive an appropriate modification of the method for the resulting magnetostatic limit. We have to stress, though, that our methods require very accurate multistatic measurements of the electromagnetic field for multiple different excitations, cf. Section 2, which can not be realized using a single off-the-shelf metal detector. Thus the applicability to field measurements still needs to be investigated.

Throughout this work we restrict ourselves to the case of penetrable dielectric or magnetic non-conducting objects in a homogeneous background. However, in the last section we will also comment on the expected effects of a layered background and of conducting objects, and show some numerical examples for these cases as well.

The outline of this paper is as follows. In Section 2 we describe our model of a metal detector and define the measurement operator M_g^ω . In Section 3 we derive the theoretical foundations for the Linear Sampling Method for penetrable objects. Sections 4 and 5 are devoted to the Factorization Method for the electrostatic and the magnetostatic limits of M_g^ω , respectively. In Section 6 we finally comment on layered media and conducting materials.

2. The setting

A simplified model of a standard metal detector is shown in Figure 1. Inside some device S , a time-harmonic current is driven through a coil of wire, thus generating a primary electromagnetic field. A second coil of wire serves as a detector for electromagnetic fields that are scattered back from objects Ω in the vicinity of the device. In order to cancel out the effects of the primary field the two coils have to be properly arranged close to each other. Thus, a simple metal detector generates only a single electromagnetic field (determined by the form of the coil), and the measurements of the scattered field are in some sense taken at the same location as the excitations (so-called *monostatic* measurements). In the following we will work with an *idealized device* that does not

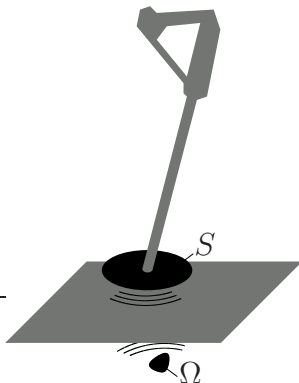


Figure 1. Simplified model of a metal detector

have these two restrictions. More precisely, we assume that we can create arbitrarily shaped surface currents in S and that for every current we can measure the (tangential component of the) scattered electric field everywhere on S . Of course, such *multistatic* measurements cannot be obtained with a single metal detector. However, one can think of this to be approximately realized with a multiarray of off-the-shelf metal detectors, cf., e.g., [3, 7, 19].

We now turn to the mathematical description of our setting. Assume that electromagnetic fields are generated by time-harmonic surface currents with complex amplitude J and frequency ω in some two-dimensional device S , where

$$S \subset \Sigma_0 := \{(x, y, 0) \in \mathbb{R}^3\}$$

is a smoothly bounded, relatively open domain. In the absence of conducting media the complex amplitudes E^ω and H^ω of the electric and magnetic components of the fields are given by Maxwell's equations

$$\operatorname{curl} H^\omega + i\omega\epsilon E^\omega = J, \quad -\operatorname{curl} E^\omega + i\omega\mu H^\omega = 0, \quad (2.1)$$

together with the radiation condition

$$\int_{\partial B_\rho} |\nu \wedge \mu H^\omega + \epsilon E^\omega|^2 \, d\sigma \rightarrow 0 \quad \text{for } \rho \rightarrow \infty. \quad (2.2)$$

Here ϵ is the dielectricity, μ is the permeability, and B_ρ the ball of radius ρ around the origin with outer normal ν . Throughout the paper, we will assume that ϵ and μ are constant outside some open bounded set Ω (the *scatterer*) with smooth boundary $\partial\Omega$ and connected complement $\mathbb{R}^3 \setminus \Omega$. Applying the usual change of units (cf., e.g., Monk [29]) we write

$$\epsilon = 1 + \epsilon_1 \chi_\Omega(x) \quad \text{and} \quad \mu = 1 + \mu_1 \chi_\Omega(x).$$

where $\epsilon_1, \mu_1 \in L^\infty(\Omega)$ have essential infima larger than -1 .

The left-hand sides of the equations in (2.1) have to be understood in the distributional sense for $E^\omega, H^\omega \in L^2_{\text{loc}}(\mathbb{R}^3)^3$. Then the second equation yields that $E^\omega \in H_{\text{loc}}(\operatorname{curl}, \mathbb{R}^3)$. Regarding the surface currents J , we assume that

$$J \in TH^{-1/2}(\operatorname{div}, S) := \{u \in TH^{-1/2}(\operatorname{div}, \Sigma_0) : u = 0 \text{ in } \Sigma_0 \setminus \overline{S}\}.$$

$TH^{-1/2}(\text{div}, S)$ can be regarded as a subset of the dual space of $H_{\text{loc}}(\text{curl}, \mathbb{R}^3)$ (and thus as a subset of the space of distributions) using the usual identification between $J \in TH^{-1/2}(\text{div}, S)$ and the mapping

$$\varphi \mapsto \int_S J \cdot \varphi|_S \, d\sigma, \quad \varphi \in H_{\text{loc}}(\text{curl}, \mathbb{R}^3),$$

where the integral is actually the dual pairing between $TH^{-1/2}(\text{div}, S)$ and its dual $TH^{-1/2}(\text{curl}, S)$. It is well known that solutions E^ω, H^ω of the homogeneous Maxwell's equations with constant dielectricity and permeability are analytic vector fields, so that the integral in (2.2) makes sense for every ball B_ρ that is large enough to contain S and the scatterer Ω . Furthermore, (2.2) is equivalent to

$$H^\omega \wedge x - |x|E^\omega \rightarrow 0 \quad \text{for } |x| \rightarrow \infty. \quad (2.3)$$

It is usually convenient to eliminate the magnetic component H^ω from (2.1) and (2.3) which leads to

$$\text{curl} \left(\frac{1}{\mu} \text{curl} E^\omega \right) - \omega^2 \epsilon E^\omega = i\omega J \quad (2.4)$$

and

$$x \wedge \text{curl} E^\omega + |x|i\omega E^\omega \rightarrow 0 \quad \text{for } |x| \rightarrow \infty, \quad (2.5)$$

where we now have to add the assumption that $E^\omega \in H_{\text{loc}}(\text{curl}, \mathbb{R}^3)$.

The solvability of this forward problem can be treated as in [29] by reducing it to a sufficiently large ball B_r and formulating exact non-local boundary conditions on the artificial boundary ∂B_r . This approach leads to a Fredholm problem, so that existence of a solution is equivalent to its uniqueness. In the following, we will assume that we are in a situation where this uniqueness is guaranteed, or in other words, that no resonances occur.

Our idealized detector not only imposes the electric current J but also measures the tangential component of the induced electric field E^ω on S . We therefore introduce the measurement operator

$$M_t^\omega : \begin{cases} TH^{-1/2}(\text{div}, S) \rightarrow TH^{-1/2}(\text{curl}, S), \\ J \mapsto \gamma_\tau E_t^\omega|_S := (e_3 \wedge E_t^\omega) \wedge e_3, \end{cases}$$

where E_t^ω solves (2.4) and (2.5) and $e_3 := (0, 0, 1)^T \in \mathbb{R}^3$. Our goal is to determine Ω from this measurement operator M_t^ω . The subscript t stands for measurements of the total field. We also introduce the measurements of the incoming or primary field, i.e., the field that would be generated in the absence of a scatterer

$$M_i^\omega : J \mapsto \gamma_\tau E_i^\omega|_S,$$

where E_i^ω solves

$$\text{curl} \text{curl} E_i^\omega - \omega^2 E_i^\omega = i\omega J$$

and satisfies the radiation condition (2.5). The Linear Sampling Method works with the difference of these two operators

$$M_s^\omega := M_t^\omega - M_i^\omega,$$

that is with measurements of the so-called secondary or scattered field $E_s^\omega := E_t^\omega - E_i^\omega$.

3. The Linear Sampling Method

The Linear Sampling Method relates the question whether a point z in the lower half space \mathbb{R}_-^3 belongs to the scatterer Ω to whether the tangential trace of a certain singular function $E_{z,d}^\omega$ belongs to the range of the measurements $\mathcal{R}(M_s^\omega)$. To be more precise let $E_{z,d}^\omega$ be the primary electric field of a point current in z directed in some arbitrary direction $d \in \mathbb{R}^3$, $|d| = 1$, i.e., the solution of

$$\operatorname{curl} \operatorname{curl} E_{z,d}^\omega - \omega^2 E_{z,d}^\omega = i\omega \delta_z d$$

together with the radiation condition (2.5). Using the outgoing fundamental solution of the Helmholtz equation

$$\Phi^\omega(x) := \frac{1}{4\pi} \frac{e^{i\omega|x-z|}}{|x-z|}$$

an explicit expression for $E_{z,d}^\omega$ is

$$E_{z,d}^\omega(x) = \Phi^\omega d + \frac{1}{\omega^2} \operatorname{grad} \operatorname{div} (\Phi^\omega d).$$

Using these singular functions the scatterer Ω can be determined from the range of the operator

$$L : TH^{-1/2}(\operatorname{div}, \partial\Omega) \rightarrow TH^{-1/2}(\operatorname{curl}, S), \quad \psi \mapsto \gamma_\tau E^\omega|_S$$

which describes the virtual measurements of applying a magnetic field ψ on the scatterer's surface $\partial\Omega$, and measuring the corresponding tangential trace $\gamma_\tau E^\omega|_S$ of the solution of the exterior problem

$$\operatorname{curl} \operatorname{curl} E^\omega - \omega^2 E^\omega = 0, \quad \nu \wedge \operatorname{curl} E^\omega|_{\partial\Omega} = \psi,$$

and the radiation condition (2.5).

Theorem 3.1. *Let $d \in \mathbb{R}^3$, $|d| = 1$ be an arbitrary direction. A point $z \in \mathbb{R}_-^3$ belongs to Ω if and only if $\gamma_\tau E_{z,d}^\omega \in \mathcal{R}(L)$.*

Proof. In [18, Theorem 6.1] this theorem is proven for the case of magnetic dipole excitations and measurements of the magnetic field in $TL^2(S)$. The present case follows from interchanging the electric and the magnetic fields and noting that both $\gamma_\tau E_{z,d}^\omega$ and functions in $\mathcal{R}(L)$ are elements of $TL^2(S)$. \square

Since the scattered field E_s^ω solves the exterior problem in the definition of L , we have the factorization

$$M_s^\omega = LG, \tag{3.1}$$

where $G : TH^{-1/2}(\text{div}, S) \rightarrow TH^{-1/2}(\text{div}, \partial\Omega)$ maps the applied surface currents J to $\nu \wedge \text{curl } E_s^\omega|_{\partial\Omega}$. G can also be restricted to $TL^2(S) \cap TH^{-1/2}(\text{div}, S)$ and then extended by continuity to a mapping

$$G : TL^2(S) \rightarrow TH^{-1/2}(\text{div}, \partial\Omega).$$

Since also $\mathcal{R}(L) \subset TL^2(S)$, one can as well consider M_s^ω as an operator from $TL^2(S)$ to $TL^2(S)$. For both realizations of M_s^ω , we obtain from Theorem 3.1 and (3.1) the key result of the Linear Sampling Method:

Corollary 3.2. *If $\gamma_\tau E_{z,d}^\omega \in \mathcal{R}(M_s^\omega)$ for some point $z \in \mathbb{R}_-^3$ (and arbitrary direction d) then $z \in \Omega$.*

Corollary 3.2 shows that the set of points $z \in \mathbb{R}_-^3$, for which $\gamma_\tau E_{z,d}^\omega \in \mathcal{R}(M_s^\omega)$ defines a (possibly empty) subset $\tilde{\Omega} \subset \Omega$. Numerically, one can use this result to choose a sample of points $z \in \mathbb{R}_-^3$ and test whether $\gamma_\tau E_{z,d}^\omega \in \mathcal{R}(M_s^\omega)$ or not.

A more common formulation of the Linear Sampling Method is obtained by searching for a solution g_z of

$$M_s^\omega g_z = \gamma_\tau E_{z,d}^\omega, \tag{3.2}$$

which is an integral equation of the first kind. If the frequency does not correspond to what is called a *transmission eigenvalue* of the object (cf. Cakoni, Fares and Haddar [8] and Kirsch [25]) then M_s^ω is a compact, injective operator with dense range, so that this equation can always be solved approximately to obtain some $g_{z,\epsilon}$ with

$$\|M_s^\omega g_{z,\epsilon} - \gamma_\tau E_{z,d}^\omega\| < \epsilon.$$

The range condition $\gamma_\tau E_{z,d}^\omega \in \mathcal{R}(M_s^\omega)$ is then equivalent to the question, whether there exists a sequence of approximate solutions $g_{z,\epsilon}$ that stays bounded as ϵ tends to zero. For $z \notin \tilde{\Omega}$ this is not possible by the above arguments, so that $g_{z,\epsilon}$ is likely to blow up when z approaches $\partial\tilde{\Omega}$.

However, we feel that two conceptual flaws of the method are somewhat disguised by this more common formulation. The first is that proper regularization (e.g., Tikhonov regularization) is needed to actually guarantee that a bounded sequence is found. The second aspect is more fundamental, namely that the distinction between $\tilde{\Omega}$ and Ω is usually ignored in the literature, and this difference is far from being well understood.

We now show some numerical results that we have obtained with the Linear Sampling Method on simulated forward data. The measurement device is a square of approximate size 32cm \times 32cm located at height $z = 5$ cm (above a virtual ground). On a 6×6 equidistant grid on this device we have imposed tangential point currents with a frequency of 20kHz and measured the tangential components of the resulting scattered electric field on the same grid. The scatterer is a dielectric ellipsoid with the electromagnetic properties of rubber ($\epsilon_1 = 2$, $\mu_1 = 0$) whose center is located 15cm below the measurement device. The coordinates of its center are $x = 2$ cm, $y = 3$ cm and $z = -10$ cm, its half-axes have the lengths 3cm, 2cm and 1cm. Figure 2 shows in the first row the three-dimensional reconstruction and a horizontal cut at $z = -10$ cm

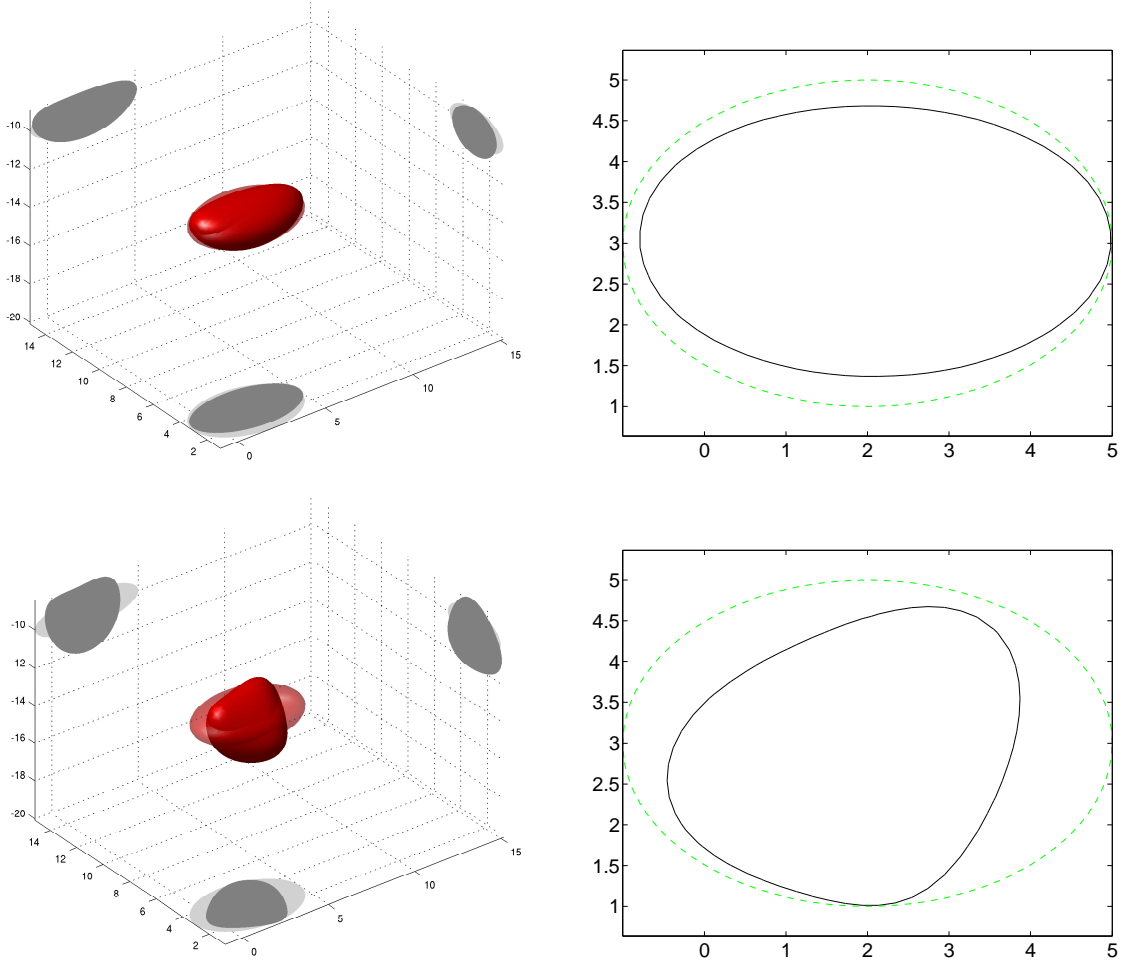


Figure 2. Reconstructions with the Linear Sampling Method

for unperturbed simulated forward data, which contains an estimated relative error of 0.1%. The second row shows the reconstruction that we obtain after perturbing the simulated data by a relative error of 1%. The true scatterer is plotted with a lighter color, resp., a dashed line, while a darker color, resp., a solid line is used for the reconstruction.

The numerical implementation is the same that had been used in [18], where also a numerical example for an object in a lossy medium is presented. Concerning implementation details we refer the interested reader to this work and the related works on factorization and linear sampling methods cited in the introduction. We note, however, that the implementation relies on calculating an approximate preimage \tilde{g}_z of equation (3.2) and checking whether its norm is *very large* (indicating that (3.2) has no solution, i.e., $\gamma_\tau E_{z,d}^\omega \notin \mathcal{R}(M_s^\omega)$). This requires the choice of an additional threshold parameter $C_\infty > 0$ to distinguish points with *very large* values $\|\tilde{g}_z\| \geq C_\infty$ from those with *small* values $\|\tilde{g}_z\| < C_\infty$. Although we have stressed that, from a theoretical point of view, there is no guarantee that the set $\tilde{\Omega}$ determined by the Linear Sampling Method is close to Ω , the choice of the threshold parameter – which up to now is done on an

empirical level – introduces some ambiguity. Tuning the parameter in an appropriate way the size of this approximation $\tilde{\Omega}$ may increase quite a bit, and with appropriate calibration the method is capable to reconstruct the true scatterer well. In the following section, we derive an explanation for this good performance which is based on the fact that our measurement setup uses a very low frequency.

4. The electrostatic limit

We now examine the asymptotic behavior of our measurements as ω tends to zero. We will restrict ourselves to a formal argumentation. For a mathematically rigorous derivation we refer the reader to the work of Ammari and Nédélec in [2], where the asymptotic expansion is carried out for the similar case of a fixed incoming wave.

We first note that (2.4) implies that

$$\operatorname{div}(\epsilon E^\omega) = \frac{1}{i\omega} \operatorname{div} J, \quad (4.1)$$

so that a part of E^ω behaves like ω^{-1} if the applied surface currents are not divergence-free. If we formally expand E^ω into a power series in ω ,

$$E^\omega = \frac{1}{\omega} E_{-1} + E_0 + O(\omega),$$

then we obtain from (2.4), (4.1), and (2.5) that E_{-1} and E_0 solve

$$\operatorname{curl} \left(\frac{1}{\mu} \operatorname{curl} E_{-1} \right) = 0, \quad \operatorname{div}(\epsilon E_{-1}) = \frac{1}{i} \operatorname{div} J, \quad (4.2)$$

$$\operatorname{curl} \left(\frac{1}{\mu} \operatorname{curl} E_0 \right) = 0, \quad \operatorname{div}(\epsilon E_0) = 0, \quad (4.3)$$

together with radiation conditions for $|x| \rightarrow \infty$

$$|x| E_{-1} \rightarrow 0, \quad x \wedge \operatorname{curl} E_{-1} \rightarrow 0, \quad (4.4)$$

$$|x| E_0 \rightarrow 0, \quad x \wedge \operatorname{curl} E_0 \rightarrow 0. \quad (4.5)$$

By multiplying (4.2) with $\overline{E_{-1}}$ and a partial integration we conclude that E_{-1} is curl-free, so that we can write it as the gradient of a scalar potential

$$\varphi \in W^1(\mathbb{R}^3) := \{u : (1 + |x|^2)^{-1/2} u \in L^2(\mathbb{R}^3), \nabla u \in L^2(\mathbb{R}^3)^3\},$$

cf., e.g., Dautray and Lions [13, IX, §1]. From (4.3) and (4.5) we obtain that $E_0 = 0$. Hence we end up with

$$E^\omega = \frac{1}{i\omega} \nabla \varphi + O(\omega), \quad (4.6)$$

where φ solves

$$\operatorname{div}(\epsilon \nabla \varphi) = \operatorname{div} J. \quad (4.7)$$

We can interpret (4.7) as the electrostatic potential φ , that is created by the surface charges $\operatorname{div} J$. We therefore introduce the measurement operator of electrostatic measurements

$$\Lambda_t : H^{-1/2}(S) \rightarrow H^{1/2}(S), \quad \rho \mapsto u|_S,$$

where u solves

$$\operatorname{div}(\epsilon \nabla u) = \rho.$$

Thus, we obtain from (4.6)

$$i\omega M_t^\omega J = \gamma_\tau \nabla \varphi|_S + O(\omega^2) = -\nabla_S \Lambda_t \nabla'_S J + O(\omega^2), \quad (4.8)$$

where

$$\nabla_S : H^{1/2}(S) \rightarrow TH^{-1/2}(\operatorname{curl}, S)$$

denotes the surface gradient on S and

$$-\nabla'_S : TH^{-1/2}(\operatorname{div}, S) \rightarrow H^{-1/2}(S)$$

the surface divergence.

Formally, it follows from our expansion that the error term in (4.8) depends continuously and linearly on J , so that the operator $-\nabla_S \Lambda_t \nabla'_S$ approximates $i\omega M_t^\omega$ up to an error of the order ω^2 . Analogously to the last section we define the measurement operators for the primary and secondary electrostatic potential Λ_i and Λ_s and obtain

$$i\omega M_s^\omega \approx -\nabla_S \Lambda_s \nabla'_S + O(\omega^2).$$

Thus for low frequencies the measurements are closely related to the electrostatic measurements Λ_s for which the Factorization Method is known to work (see Hähner [21] for the case of a grounded object, or [15] for the penetrating case). Therefore the good performance of the Linear Sampling Method can be explained by the fact that it agrees with the Factorization Method up to a term of order ω^2 that is below the measurement error.

It remains to show that the Factorization Method really works for the operator $\nabla_S \Lambda_s \nabla'_S$ and that its test functions are the low-frequency limits of those of the Linear Sampling Method. To this end let L_{ES} be the electrostatic virtual measurement operator, that maps the normal component g of an electrostatic field on the boundary of the scatterer to the resulting electrostatic potential on the measurement device, i.e.,

$$L_{\text{ES}} : H_\diamond^{-1/2}(\partial\Omega) \rightarrow H^{1/2}(S), \quad g \mapsto u|_S,$$

where the subscript " \diamond " denotes the space of functions with vanishing integral mean on each connected component of $\partial\Omega$ and $u \in W^1(\mathbb{R}^3 \setminus \overline{\Omega})$ solves

$$\Delta u = 0 \quad \text{in } \mathbb{R}^3 \setminus \overline{\Omega}, \quad \partial_\nu u|_{\partial\Omega} = g.$$

Then the points inside the scatterer Ω can be characterized by $\mathcal{R}(\nabla_S L_{\text{ES}})$ using the low frequency-limit of $E_{z,d}^\omega$.

Theorem 4.1. *Let $z \in \mathbb{R}_-^3$ be a point in the lower half space, let $d \in \mathbb{R}^3$, $|d| = 1$ be an arbitrary direction and let*

$$E_{z,d} := \operatorname{grad} \operatorname{div} \frac{d}{|x - z|}$$

be the electrostatic field of a dipole in z with direction d . Then

$$\gamma_\tau E_{z,d} \in \mathcal{R}(\nabla_S L_{\text{ES}}) \quad \text{if and only if} \quad z \in \Omega.$$

Proof. If $z \in \Omega$ then obviously

$$\gamma_\tau E_{z,d} = \nabla_S L_{\text{ES}} \left(\partial_\nu \left(\operatorname{div} \frac{d}{|x-z|} \right) \Big|_{\partial\Omega} \right) \in \mathcal{R}(\nabla_S L_{\text{ES}}).$$

Now assume that $\gamma_\tau E_{z,d} \in \mathcal{R}(\nabla_S L_{\text{ES}})$. Then there exists $u \in W^1(\mathbb{R}^3 \setminus \overline{\Omega})$ such that $\Delta u = 0$ in $\mathbb{R}^3 \setminus \overline{\Omega}$ and

$$\nabla_S u|_S = \nabla_S \operatorname{div} \frac{d}{|x-z|}.$$

u and $\operatorname{div} \frac{d}{|x-z|}$ are harmonic functions in $\mathbb{R}^3 \setminus (\overline{\Omega} \cup \{z\})$, so in particular the tangential components of $\nabla u - \nabla \operatorname{div} \frac{d}{|x-z|}$ are analytic on Σ_0 and thus vanish on Σ_0 . Since $u - \operatorname{div} \frac{d}{|x-z|}$ is harmonic on \mathbb{R}_+^3 , it follows that $u - \operatorname{div} \frac{d}{|x-z|}$ is constant on \mathbb{R}_+^3 (actually it is zero). Now the analyticity on $\mathbb{R}^3 \setminus (\overline{\Omega} \cup \{z\})$ yields that $u - \operatorname{div} \frac{d}{|x-z|}$ must be constant on $\mathbb{R}^3 \setminus (\overline{\Omega} \cup \{z\})$. But u is square integrable in any bounded subset of $\mathbb{R}^3 \setminus \Omega$, while $\operatorname{div} \frac{d}{|x-z|}$ is only square integrable if $z \in \Omega$. \square

For the electrostatic measurements a factorization result that relates Λ_s to L_{ES} is already known.

Theorem 4.2. Λ_s can be factorized into

$$\Lambda_s = L_{\text{ES}} F L'_{\text{ES}},$$

with a symmetric operator $F : H_\diamond^{1/2}(\partial\Omega) \rightarrow H_\diamond^{-1/2}(\partial\Omega)$. If $\epsilon_1 < 0$ (in the sense of essential supremum) then F is coercive, if $\epsilon_1 > 0$ (in the sense of essential infimum) then $-F$ is coercive.

Proof. This is shown for closed surfaces in [15, Sect. 4.4] and holds with the same proof also in the present case. \square

Theorem 4.3. Let $\epsilon_1 < 0$ or $\epsilon_1 > 0$ and denote by

$$\iota : TH^{-1/2}(\operatorname{div}, S) \rightarrow TH^{-1/2}(\operatorname{curl}, S)$$

the Riesz isomorphism that identifies the Hilbert space $TH^{-1/2}(\operatorname{div}, S)$ with its dual. Then

$$\mathcal{R}(|\nabla_S \Lambda_s \nabla'_S \iota^{-1}|^{1/2}) = \mathcal{R}(\nabla_S L_{\text{ES}}).$$

Proof. This follows from the standard functional analytic arguments for the Factorization Method (cf., e.g., [15, Lemma 3.5]). \square

Just like M_s^ω the operator $\nabla_S \Lambda_s \nabla'_S$ can also be considered as a mapping from $TL^2(S)$ to $TL^2(S)$, so that it seems more natural to take the square root in this space instead of using the above Riesz isomorphism. The following functional analytic result shows that our range test can indeed be formulated this way.

Theorem 4.4. *Let V, W be two Hilbert spaces such that $V \cap W$ is dense in V as well as in W . Furthermore let*

$$A : V \rightarrow V' \quad \text{and} \quad B : W \rightarrow W'$$

be two continuous, symmetric and positive linear operators, that coincide on $V \cap W$.

Then for every $y \in V' \cap W'$ we have

$$y \in \mathcal{R}((A\iota_V^{-1})^{1/2}) \quad \text{if and only if} \quad y \in \mathcal{R}((B\iota_W^{-1})^{1/2}),$$

where ι_V and ι_W are the Riesz isomorphisms that identify V and V' , and W and W' , respectively.

Proof. We first note that because of the denseness of $V \cap W$, the spaces V' and W' can both be identified with subspaces of the larger space $(V \cap W)'$, so that it makes sense to speak of $V' \cap W'$.

Let $y \in V' \cap W'$. A well-known functional analytic result (cf., e.g., [14, Lemma 3.4] for an elementary proof) is that $y \in \mathcal{R}((A\iota_V^{-1})^{1/2})$ is equivalent to the existence of a $C > 0$ such that

$$\langle y, x \rangle \leq C \|((A\iota_V^{-1})^{1/2})'x\| \quad \text{for all } x \in V.$$

Since both sides are continuous with respect to $x \in V$, this is equivalent to

$$\langle y, x \rangle \leq C \|((A\iota_V^{-1})^{1/2})'x\| = C \langle A'x, x \rangle = C \langle B'x, x \rangle = C \|((B\iota_W^{-1})^{1/2})'x\|$$

for all $x \in V \cap W$. From the continuity with respect to $x \in W$ this is now equivalent to

$$\langle y, x \rangle \leq C \|((B\iota_W^{-1})^{1/2})'x\| \quad \text{for all } x \in W,$$

and thus to $y \in \mathcal{R}((B\iota_W^{-1})^{1/2})$. \square

Since the traces of the singular test functions $\gamma_\tau E_{z,d}$ are elements of $TL^2(S)$ as well as of $TH^{-1/2}(\text{curl}, S)$ we obtain from Theorem 4.3 and 4.4 the following.

Corollary 4.5. *Let $\epsilon_1 < 0$ or $\epsilon_1 > 0$. For every point $z \in \mathbb{R}_-^3$ and every direction $d \in \mathbb{R}^3$, $|d| = 1$*

$$\gamma_\tau E_{z,d} \in \mathcal{R}(|\nabla_S \Lambda_s \nabla'_S|^{1/2}) \quad \text{if and only if} \quad z \in \Omega,$$

where the square root is taken with respect to $TL^2(S)$.

Thus Ω can be found by considering M_s^ω as an approximation to $\nabla_S \Lambda_s \nabla'_S$ and by testing for a sample of points $z \in \mathbb{R}_-^3$ whether $\gamma_\tau E_{z,d} \in \mathcal{R}(|M_s^\omega|^{1/2})$. The numerical results that we have achieved with the factorization method on the same forward data as in Section 3 are shown in Figure 3 (using the same color and line codes as in Figure 2). Note that the test function $E_{z,d}$ is essentially the same as $E_{z,d}^\omega$ for low frequencies. A more substantial difference to the Linear Sampling Method in Section 3 is the use of the square root operator $|M_s^\omega|^{1/2}$ instead of M_s^ω . Nonetheless, we have observed that a suitable calibration of the threshold in the Linear Sampling Method, cf. Section 3, yields reconstructions of about the same quality as the Factorization Method. (Again we refer to [18] for the details of this implementation.) However, the method described

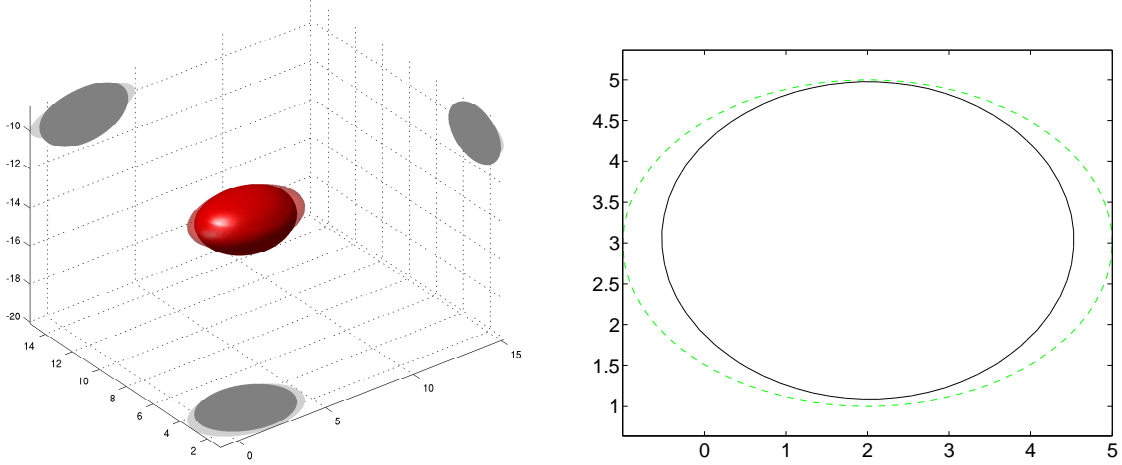


Figure 3. Reconstructions with the Factorization Method for electrostatics

in this Section is based on the rigorously justified Factorization Method, thus giving an explanation for the previously observed good performance of the Linear Sampling Method.

5. The magnetostatic limit

In the last section we compared the Linear Sampling Method to the Factorization Method for the electrostatic limit. This requires the use of applied currents with non-zero divergence, i.e., the presence of surface charges. In practical situations one will have to work with divergence-free currents, e.g., currents that are applied along closed coils. We show in this section how the argumentation and especially the test functions must be modified to deal with this situation.

For divergence-free currents the terms E_{-1} and E_0 from the formal asymptotic expansion of E^ω in Section 4 vanish, and so

$$E^\omega = \omega E_1 + \omega^2 E_2 + O(\omega^3).$$

For E_1 and E_2 we obtain from (2.4), (4.1), and (2.5)

$$\operatorname{curl} \left(\frac{1}{\mu} \operatorname{curl} E_1 \right) = iJ, \quad \operatorname{div} (\epsilon E_1) = 0, \quad (5.1)$$

$$\operatorname{curl} \left(\frac{1}{\mu} \operatorname{curl} E_2 \right) = 0, \quad \operatorname{div} (\epsilon E_2) = 0, \quad (5.2)$$

with the radiation conditions for $|x| \rightarrow \infty$

$$|x| E_1 \rightarrow 0, \quad x \wedge \operatorname{curl} E_1 \rightarrow 0, \quad (5.3)$$

$$|x| E_2 \rightarrow 0, \quad x \wedge \operatorname{curl} E_2 \rightarrow 0. \quad (5.4)$$

We conclude that $E_2 = 0$, so that

$$E^\omega = i\omega E + O(\omega^3),$$

where $E = -iE_1$ solves

$$\operatorname{curl}\left(\frac{1}{\mu}\operatorname{curl}E\right) = J, \quad \operatorname{div}(\epsilon E) = 0. \quad (5.5)$$

This can be interpreted as the magnetostatic field $\operatorname{curl}E$, resp. its vector potential E , that is created by (stationary) currents J . To define the magnetostatic measurements M_t , we denote by $TL_\diamond^2(S)$ the subspace of divergence-free currents in $TL^2(S)$ and let

$$M_t : TL_\diamond^2(S) \rightarrow TL_\diamond^2(S)'$$

be the operator that maps an applied current J to the tangential trace $\gamma_\tau E$ of the solution $E \in W^1(\mathbb{R}^3)^3$ of (5.5). The dual space $TL_\diamond^2(S)'$ is the quotient space of $TL^2(S)$ modulo the closure of the space of tangential traces of gradient fields on S with respect to $TL^2(S)$. This corresponds to the fact that gradient fields are integrated to zero along closed coils. Another consequence of factoring out gradient fields is that M_t does not change if $\operatorname{div}(\epsilon E) = 0$ is replaced by $\operatorname{div}E = 0$ in (5.5), so that the measurements do not depend on the dielectricity, just like the electrostatic measurements did not depend on the permeability.

Analogously to the two previous sections we define M_i as measurements without an object and M_s as the difference of M_t and M_i . Then our formal asymptotic analysis suggests that up to a relative error of the order of ω^2

$$M_s^\omega \approx i\omega M_s.$$

We note that this asymptotic result can not only be made rigorous but it can also be shown that (even without further smoothness assumptions on μ_1 and ϵ_1) Maxwell's equations are uniquely solvable for sufficiently small frequencies ω , see [17]. This justifies our somewhat sloppy assumption of being in a situation where uniqueness is guaranteed.

We now proceed along the lines of the last section and introduce the magnetostatic virtual measurement operator

$$L_{\text{MS}} : \psi \mapsto \gamma_\tau E, \quad (5.6)$$

where E solves

$$\operatorname{curl}\operatorname{curl}E = 0 \quad \text{in } \mathbb{R}^3 \setminus \overline{\Omega}, \quad (5.7)$$

$$\operatorname{div}E = 0 \quad \text{in } \mathbb{R}^3 \setminus \overline{\Omega}, \quad (5.8)$$

$$\nu \wedge \operatorname{curl}E|_{\partial\Omega} = \psi, \quad (5.9)$$

$$\nu \cdot E|_{\partial\Omega} = 0. \quad (5.10)$$

The choice of adequate function spaces for L_{MS} is more involved than in the previous sections. For this reason the proofs of the following three theorems can be found in the Appendix.

Theorem 5.1. *Equations (5.6)–(5.10) define a continuous linear operator*

$$L_{\text{MS}} : TH_\diamond^{-1/2}(\partial\Omega) \rightarrow TL_\diamond^2(S)',$$

where $TH_\diamond^{-1/2}(\partial\Omega)$ is the closure of $\overrightarrow{\operatorname{curl}}|_{\partial\Omega}(H^{1/2}(\partial\Omega))$ in $TH^{-1/2}(\partial\Omega)$, $\overrightarrow{\operatorname{curl}}|_{\partial\Omega}$ denoting the surface curl (cf., e.g., Cessenat [10, Chp. 2]).

The points inside the scatterer can now be characterized using (a vector potential of) the magnetic field of a magnetic dipole in a point z with direction d ,

$$G_{z,d}(x) := \operatorname{curl} \frac{d}{|x-z|}.$$

Theorem 5.2. *Let $z \in \mathbb{R}_-^3$ and $d \in \mathbb{R}^3$, $|d| = 1$ be an arbitrary direction. Then*

$$\gamma_\tau G_{z,d} \in \mathcal{R}(L_{\text{MS}}) \quad \text{if and only if} \quad z \in \Omega.$$

Our magnetostatic measurements are closely related to the vector harmonic equations for which Kress has proven in [26, 27] that the Factorization Method works. We now show that this is also the case here, i.e., that we can calculate the range of L_{MS} from our measurements M_s .

Theorem 5.3. *Let $\mu_1 < 0$ or $\mu_1 > 0$ and ι denote the Riesz isomorphism from $TL_\diamond^2(S)$ to its dual. Then*

$$\mathcal{R}(|M_s \iota^{-1}|^{1/2}) = \mathcal{R}(L).$$

Identifying $TL_\diamond^2(S)$ with its dual we finally conclude from Theorem 5.2 and 5.3 the following.

Corollary 5.4. *Let $\mu_1 < 0$ or $\mu_1 > 0$. For every point $z \in \mathbb{R}_-^3$ and every direction $d \in \mathbb{R}^3$, $|d| = 1$,*

$$\gamma_\tau G_{z,d} \in \mathcal{R}(|M_s|^{1/2}) \quad \text{if and only if} \quad z \in \Omega.$$

Thus in the case of divergence-free currents we can locate Ω by considering M_s^ω as an approximation to the magnetostatic measurements M_s , and consequently use the magnetostatic singular function $G_{z,d}$ for the range tests.

We have tested this method numerically with a similar setting as in the two previous sections. Divergence-free currents with a frequency of 20kHz have been simulated by imposing normal magnetic dipoles on an equidistant 12×12 grid of normal excitations on the same measurement device S as in Section 3. Note that in comparison to the previously used 6×6 grid of tangential excitations, this increases the number of discrete measurements from a 72×72 matrix to a 144×144 matrix, which we have observed to be necessary to obtain a comparable quality to the previous sections. This may indicate a higher degree of ill-posedness for the magnetostatic setting than for the electrostatic one, however, such a conclusion should be treated with care as the data are different, too.

The scatterer is the same ellipsoid as in the two previous sections, but we now use a ferromagnetic material with the permeability of iron ($\epsilon_1 = 0$, $\mu_1 = 299$) and a diamagnetic material with the permeability of copper ($\epsilon_1 = 0$, $\mu_1 = -6.4 \cdot 10^{-6}$).

Figure 4 shows the three-dimensional reconstruction and a horizontal cut at $z = -10\text{cm}$ for the ferromagnetic case (top row) and the diamagnetic case (second row). Again, the true scatterer is plotted with a lighter color, resp., a dashed line, while a darker color, resp., a solid line is used for the reconstruction. The quality of the results is comparable to each other and to that of the electrostatic case.

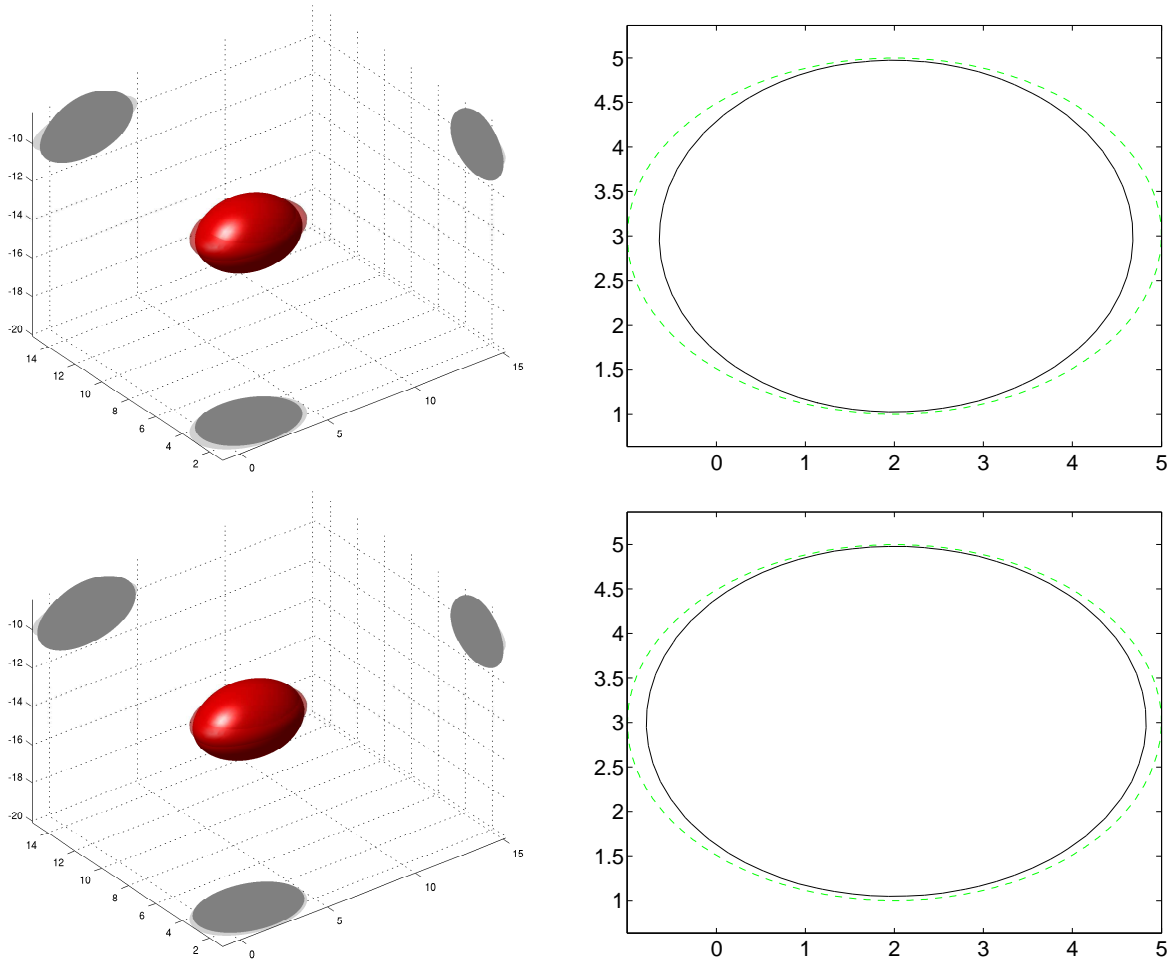


Figure 4. Reconstructions with the Factorization Method for magnetostatics

6. Outlook on layered background and conducting objects

So far, our theory does not cover the important cases of conducting objects and of objects in a layered background. In this section we try to justify why we expect that the theory can (at least partly) be extended to these cases and show some promising numerical examples. We restrict ourselves to the practically relevant case of divergence-free currents studied in Section 5.

Concerning the case of a layered background we recall that we have seen in Section 5, that for low frequencies the measurements became independent of the dielectricity ϵ . Consequently, the Factorization Method in Section 5 does also work if the object is hidden in some other (unknown!) dielectric medium, e.g., if a magnetic object is buried in humid earth. Though our asymptotic analysis was based on the assumption that ϵ equals 1 outside some bounded domain, we expect that this also holds for the case of a *layered medium*, i.e., when $\epsilon \neq 1$ in a half space below the measurement device S .

Concerning objects with a finite conductivity σ on the other side, Maxwell's equation (2.4) has to be supplemented with a term describing the induced currents

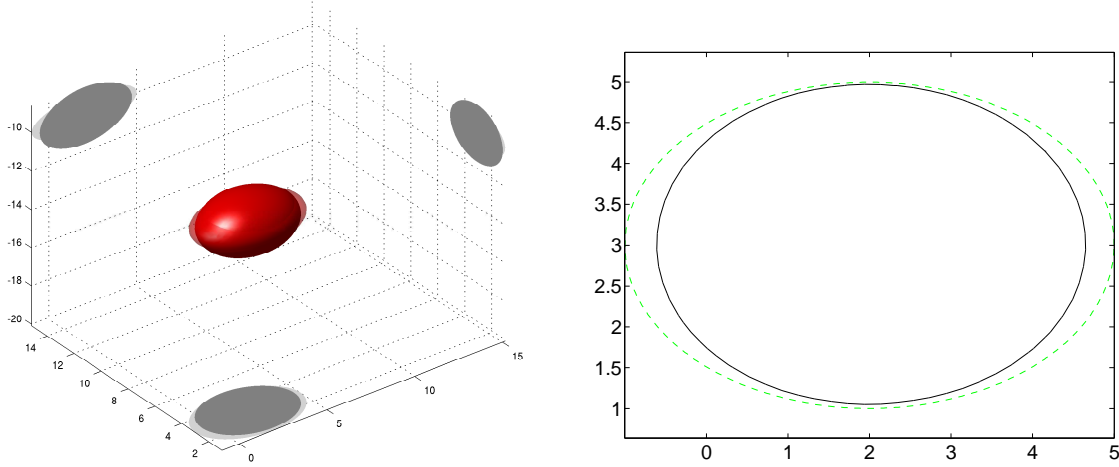


Figure 5. Reconstruction of a conducting diamagnetic object in a dielectric halfspace

in the object, i.e.,

$$\operatorname{curl} \left(\frac{1}{\mu} \operatorname{curl} E^\omega \right) - \omega^2 \epsilon E^\omega = i\omega(J + \sigma E^\omega).$$

In [1], Ammari, Buffa and Nédélec showed that for low frequencies the (inverse) Fourier transform of E^ω , i.e., the time-dependent electric field, can be approximated by the solution $E(x, t)$ of

$$\partial_t(\sigma E) - \operatorname{curl} \left(\frac{1}{\mu} \operatorname{curl} E \right) = -\partial_t \mathcal{J}, \quad (6.1)$$

where \mathcal{J} is the (inverse) Fourier transform of J , i.e., the time-dependent applied currents. Equation (6.1) is parabolic inside the object (where $\sigma > 0$) and elliptic outside (where $\sigma = 0$). The physical interpretation of (6.1) is that inside the object the electric field takes some time to build up due to eddy currents, while on the outside it almost instantly reaches a stationary state. A scalar model problem for this situation is to consider the temperature u of a domain with no (or very low) heat capacity ($c \approx 0$) that has inclusions with a high heat capacity $c > 0$, i.e.,

$$\partial_t(cu) - \operatorname{div}(\kappa \operatorname{grad} u) = 0,$$

cf. [16] for a rigorous derivation of this model. Within this model the inclusions take some time to heat up, while the background medium is always in a state of thermal equilibrium. Under the assumption that the thermal conductivity κ of the inclusions is higher than that of the background, it was shown in [14] that the Factorization Method also works for this parabolic-elliptic situation. The magnetostatic analog to the thermal conductivity κ is the term $1/\mu$. We expect that the arguments in [14] can be extended to the vector-valued case considered in this work, so that the method in Section 5 can also be used to detect diamagnetic, conducting objects (e.g. copper).

Figure 5 shows the numerical reconstruction for the method and the geometry from Section 5 applied to an ellipsoidal diamagnetic conducting scatterer with the properties

of copper ($\epsilon_1 = 0$, $\mu_1 = -6.4 \cdot 10^{-6}$, $\sigma = 5.8 \cdot 10^7$) in a dielectric halfspace with the dielectricity of air ($\epsilon = 1$ for $z > 0$), resp., humid earth ($\epsilon = 29$ for $z < 0$). Color and line codes are the same as in all previous figures, and the results again have comparable quality.

7. Conclusion

Our theoretical results and numerical examples show that the Factorization Method can be used to detect objects from electromagnetic measurements in the low-frequency regime. These results can also be used to explain the good performance of the Linear Sampling Method near the electrostatic limit observed earlier. Moreover, they reveal necessary modifications for the physically relevant setting near the magnetostatic limit. Numerical results suggest that the method can also be used to find conducting objects in a dielectric layered background.

Our results are derived for an idealized setting with multistatic measurements, and their relevance for practical applications depends heavily on the accuracy with which measurements can be taken in real life. Still, we believe that this work demonstrates a promising potential of sampling methods for a severely ill-posed problem in low-frequency electromagnetic imaging. To support our argument we refer interested readers to the recent work [4] where the Factorization Method has been applied successfully to laboratory data for a similar problem in electrical impedance tomography.

Acknowledgments

This work was motivated and partially supported by the German Federal Ministry of Education and Research in the BMBF-project "HuMin/MD – Metal detectors for humanitarian demining – Development potentials in data analysis methodology and measurement".

The authors like to thank Roland Potthast and his group at the University of Göttingen, in particular Klaus Erhard and Jochen Schulz, for generating simulated data to test our method.

Appendix

Proof of Theorem 5.1. Denote by $W_\diamond^1(\mathbb{R}^3 \setminus \overline{\Omega})^3$ the space of all $W^1(\mathbb{R}^3 \setminus \overline{\Omega})^3$ -functions with vanishing divergence and vanishing normal component on $\partial\Omega$. An equivalent variational formulation for (5.7)–(5.10) is that $E \in W_\diamond^1(\mathbb{R}^3 \setminus \overline{\Omega})^3$ solves

$$a_Q(E, v) := \int_{\mathbb{R}^3 \setminus \overline{\Omega}} \operatorname{curl} E \cdot \operatorname{curl} v \, dx = \int_{\partial\Omega} \psi \cdot \gamma_\tau v|_{\partial\Omega} \, d\sigma, \quad (\text{A.1})$$

for all $v \in W_\diamond^1(\mathbb{R}^3 \setminus \overline{\Omega})^3$, where the integral on the right hand side is again actually the dual pairing between $TH^{-1/2}(\operatorname{div}, \partial\Omega)$ and $TH^{-1/2}(\operatorname{curl}, \partial\Omega)$. In the proof of Theorem 5.3 below we will make use of the general framework for the Factorization

Method developed in [15] and the notations therein. It is in view of this notations that we introduce $Q := \mathbb{R}^3 \setminus \overline{\Omega}$, and add an index Q for quantities associated with this set. Due to our choice of $TH_\diamond^{-1/2}(\partial\Omega)$ both sides of (A.1) vanish if v is curl-free. Thus (A.1) is also well-defined on the quotient space

$$H(Q) := W_\diamond^1(\mathbb{R}^3 \setminus \overline{\Omega})^3 / \{u \in W_\diamond^1(\mathbb{R}^3 \setminus \overline{\Omega})^3 : \text{curl } u = 0\}.$$

A standard result on the relation between gradient, divergence, and curl of a vector field (cf., e.g., Dautray and Lions [13, IX, §1, Thm. 3, Rem. 1]) yields the existence of a constant $C > 0$ such that

$$\int_{\mathbb{R}^3 \setminus \overline{\Omega}} |\nabla v|^2 \, dx \leq \int_{\mathbb{R}^3 \setminus \overline{\Omega}} |\text{curl } v|^2 \, dx + C \int_{\partial\Omega} |\gamma_\tau v|^2 \, d\sigma$$

for all $v \in W_\diamond^1(\mathbb{R}^3 \setminus \overline{\Omega})^3$. Thus, a_Q is a compact perturbation of a coercive bilinear form in $W_\diamond^1(\mathbb{R}^3 \setminus \overline{\Omega})^3$. Since a_Q is also positive and its kernel is factored out in $H(Q)$, it follows that a_Q is coercive on $H(Q)$. The assertion now follows from the Lax-Milgram Theorem. \square

Proof of Theorem 5.2. The proof is similar to that of Theorem 4.1. For points $z \in \Omega$ we have that

$$\nu \wedge \text{curl } G_{z,d}|_{\partial\Omega} = \overrightarrow{\text{curl}}_{\partial\Omega} \text{div} \frac{d}{|x-z|} \in TH_\diamond^{-1/2}(\partial\Omega),$$

and using a $\varphi \in W^1(\mathbb{R}^3 \setminus \overline{\Omega})$ with

$$\Delta\varphi = 0 \quad \text{and} \quad \partial_\nu \varphi|_{\partial\Omega} = \nu \cdot G_{z,d}|_{\partial\Omega}$$

we obtain that $G_{z,d} - \nabla\varphi$ solves (5.7)–(5.10). Thus

$$\gamma_\tau G_{z,d} = L_{\text{MS}}(\nu \wedge \text{curl } G_{z,d}|_{\partial\Omega}) \in \mathcal{R}(L_{\text{MS}}).$$

On the other hand if $\gamma_\tau G_{z,d} \in \mathcal{R}(L_{\text{MS}})$ then there exists a potential E that solves (5.7)–(5.10) and $\gamma_\tau E$ coincides with $\gamma_\tau G_{z,d}$ in the quotient space $TL_\diamond^2(S)'$. From this we deduce that

$$w := \text{curl}(E - G_{z,d})$$

is a function with harmonic components, whose normal component vanishes on S . By analytic continuation the normal component has to vanish on the whole of Σ_0 . We now use a mirroring argument to show that w has to vanish in the upper half space \mathbb{R}_+^3 . To this end we define

$$\tilde{w}(x) := \begin{cases} w(x) & \text{for } x \cdot e_3 \geq 0 \\ \alpha(w(\alpha(x))) & \text{for } x \cdot e_3 < 0 \end{cases},$$

where $\alpha(x) := x - 2(x \cdot e_3)e_3$. Then one can easily check that

$$\tilde{w} \in L^2(\mathbb{R}^3)^3, \quad \text{div } \tilde{w} = 0, \quad \text{and} \quad \text{curl } \tilde{w} = 0,$$

from which we obtain that $\tilde{w} = 0$ and thus $w|_{\mathbb{R}_+^3} = 0$. Using analytic continuation again it follows that w vanishes in $\mathbb{R}^3 \setminus (\overline{\Omega} \cup \{z\})$, and as in Theorem 4.1 this yields that $z \in \Omega$. \square

Proof of Theorem 5.3. We use the general framework in [15] and therefore adapt the notations therein. Let $H(B)$ denote the space of divergence-free functions from $W^1(\mathbb{R}^3)^3$. a_Q and $H(Q)$ are defined as in the proof of Theorem 5.1. $H(\Omega)$ is defined analogously to $H(Q)$ and $a_{\Omega,0}$, $a_{\Omega,1}$ are the bilinear forms

$$\begin{aligned} a_{\Omega,0}(u, v) &= \int_{\Omega} \operatorname{curl} u \cdot \operatorname{curl} v \, dx, \\ a_{\Omega,1}(u, v) &= \int_{\Omega} \frac{1}{\mu} \operatorname{curl} u \cdot \operatorname{curl} v \, dx, \quad u, v \in H(\Omega). \end{aligned}$$

With the same arguments as in the proof of Theorem 5.1 it follows that $a_{\Omega,0}$ and $a_{\Omega,1}$ are coercive on $H(\Omega)$, assumption (V1) in [15] is fulfilled and for $\mu_1 < 0$ resp. $\mu_1 > 0$ the difference $a_{\Omega,1} - a_{\Omega,0}$ resp. $a_{\Omega,0} - a_{\Omega,1}$ is coercive on $H(\Omega)$.

With $\Sigma := \partial\Omega$ we define $H(\Sigma)$ as the dual of $TH_{\diamond}^{-1/2}(\partial\Omega)$, i.e., the quotient space of $TH^{1/2}(\partial\Omega)$ modulo its subspace of $\operatorname{curl}_{\partial\Omega}$ -free functions and $H(S) := TL_{\diamond}^2(S)'$. The restrictions $E_{(\cdot)}$ and trace operators $\gamma_{(\cdot)}$ between these spaces

$$\begin{aligned} \gamma_{Q \rightarrow S} : H(Q) &\rightarrow H(S), & E_Q : H(B) &\rightarrow H(Q), \\ \gamma_{Q \rightarrow \Sigma} : H(Q) &\rightarrow H(\Sigma), & E_{\Omega} : H(B) &\rightarrow H(\Omega), \\ \gamma_{\Omega \rightarrow \Sigma} : H(\Omega) &\rightarrow H(\Sigma) \end{aligned}$$

are then defined by adding appropriate gradients of harmonic scalar functions to obtain vanishing normal traces as in the the proof of Theorem 5.2. From [13, IX, §1, Rem. 8] we obtain that $\gamma_{Q \rightarrow \Sigma}$ and $\gamma_{\Omega \rightarrow \Sigma}$ possess continuous right inverses, so that (V3) in [15] holds. Since we have already ensured the coerciveness of the bilinear forms, the assertion follows from [15, Thm. 3.1], if we can also show (V2*) in [15], i.e., that two functions in $H(Q)$ and $H(\Omega)$ can be combined to a function in $H(B)$ if and only if their traces agree in $H(\Sigma)$. The fact that

$$\gamma_{Q \rightarrow \Sigma} E_Q u = \gamma_{\Omega \rightarrow \Sigma} E_{\Omega} \quad \text{for all } u \in H(B)$$

immediately follows from the definition of the space $H(\Sigma)$. For the other implication we have to show that each vector field u with

$$\begin{aligned} u|_{\mathbb{R}^3 \setminus \overline{\Omega}} &\in W^1(\mathbb{R}^3 \setminus \overline{\Omega})^3, \quad u|_{\Omega} \in W^1(\Omega)^3, \quad \operatorname{div} u = 0 \text{ in } \mathbb{R}^3 \setminus \partial\Omega, \\ \nu \cdot u|_{\partial\Omega^-} &= \nu \cdot u|_{\partial\Omega^+} = 0 \quad \text{and} \quad \operatorname{curl}_{\partial\Omega}(\gamma_{\tau} u|_{\partial\Omega^-} - \gamma_{\tau} u|_{\partial\Omega^+}) = 0 \end{aligned}$$

differs from a divergence-free $W^1(\mathbb{R}^3)^3$ -function only by a function with vanishing curl on $\mathbb{R}^3 \setminus \partial\Omega$. This can be proven by choosing $u - \operatorname{curl} v$, where $v \in W^1(\mathbb{R}^3)^3$ solves

$$\operatorname{curl} \operatorname{curl} v = 0 \quad \text{in } \mathbb{R}^3 \setminus \partial\Omega$$

and $\gamma_{\tau}(\operatorname{curl} v)|_{\partial\Omega^-} - \gamma_{\tau}(\operatorname{curl} v)|_{\partial\Omega^+} = \gamma_{\tau} u|_{\partial\Omega^-} - \gamma_{\tau} u|_{\partial\Omega^+}$. For the technical details of the above argumentation we refer to [17]. \square

References

- [1] Ammari H, Buffa A and Nédélec J-C 2000 A justification of eddy currents model for the Maxwell equations *SIAM J. Appl. Math.* **60** 1805–1823

- [2] Ammari H and Nédélec J-C 2000 Low-frequency electromagnetic scattering *SIAM J. Math. Anal.* **31** 836–861
- [3] Anderson J, Nordman C, Tondra M, Schneider R W and Sinclair R A 2002 Magnetic Anomaly Sensing for Landmine Alternative Systems, presented at the 2002 Mines, Demolition and Non-Lethal Conference & Exhibition, available online at <http://www.dtic.mil/ndia/2002mines/anderson.pdf>.
- [4] Azzouz M, Hanke M, Oesterlein C and Schilcher K 2007 The factorization method for electrical impedance tomography data from a new planar device *International Journal of Biomedical Imaging* vol. 2007 Article ID 83016, 7 pages, doi:10.1155/2007/83016.
- [5] Brühl M and Hanke M 2000 Numerical implementation of two noniterative methods for locating inclusions by impedance tomography *Inverse Problems* **16** 1029–1042
- [6] Brühl M 2001 Explicit characterization of inclusions in electrical impedance tomography *SIAM J. Math. Anal.* **32** 1327–1341
- [7] Bruschini C 2000 Metal Detectors in Civil Engineering and Humanitarian Demining: Overview and Tests of a Commercial Visualizing System *INSIGHT - Non-Destructive Testing and Condition Monitoring* **42**(2) 89–97.
- [8] Cakoni F, Fares M and Haddar H 2006 Analysis of two linear sampling methods applied to electromagnetic imaging of buried objects *Inverse Probl.* **22** 845–867
- [9] Cheney M, Isaacson D and Newell J C 1999 Electrical Impedance Tomography *SIAM Rev.* **41** 85–101
- [10] Cessenat M 1996 *Mathematical Methods in Electromagnetism* (Singapore: World Scientific)
- [11] Colton D and Kirsch A 1996 A simple method for solving inverse scattering problems in the resonance region *Inverse Problems* **12** 383–393
- [12] Colton D and Kress R 2006 Using fundamental solutions in inverse scattering *Inverse Problems* **22** R49–R66
- [13] Dautray R and Lions J L 2000 *Mathematical Analysis and Numerical Methods for Science and Technology - Volume 3: Spectral Theory and Applications* (Berlin: Springer-Verlag).
- [14] Frühauf F, Gebauer B and Scherzer O 2007 Detecting interfaces in a parabolic-elliptic problem from surface measurements *SIAM J. Numer. Anal.* **45** 810–836
- [15] Gebauer B 2006 The factorization method for real elliptic problems, *Z. Anal. Anwend.* **25** 81–102
- [16] Gebauer B 2007 Sensitivity analysis of a parabolic-elliptic problem, *Quart. Appl. Math.* **65** 591–604
- [17] Gebauer B 2006 Gebietserkennung mit der Faktorisierungsmethode *Dissertation* Universität Mainz <http://nbn-resolving.de/urn/resolver.pl?urn=urn:nbn:de:hebis:77-11370>
- [18] Gebauer B, Hanke M, Kirsch A, Muniz W and Schneider C 2005 A sampling method for detecting buried objects using electromagnetic scattering *Inverse Problems* **21** 2035–2050
- [19] Geneva International Centre for Humanitarian Demining (GICHD) 2005 *Metal Detectors and PPE Catalogue 2005*, Geneva, ISBN 2-88487-024-5
- [20] Hanke M and Brühl M 2003 Recent progress in electrical impedance tomography *Inverse Problems* **19** S65–90
- [21] Hähner P 1999 An inverse Problem in electrostatics *Inverse Problems* **15** 961–975
- [22] Kirsch A 1998 Characterization of the shape of the scattering obstacle using the spectral data of the far field operator *Inverse Problems* **14** 1489–512
- [23] Kirsch A 2004 The factorization method for Maxwell’s equations *Inverse Problems* **20** S117–134
- [24] Kirsch A 2007 An integral equation for Maxwell’s equations in a layered medium with an application to the Factorization Method *J. Integral Equations Appl.* **19** 333–358
- [25] Kirsch A 2007 An integral equation approach and the interior transmission problem for Maxwell’s equations *Inverse Problems and Imaging* **1** 107–127
- [26] Kress R 2002 A sampling method for an inverse boundary value problem for harmonic vector fields in *Ill-Posed and Inverse Problems*, S I Kabanikhin and V G Romanov, eds. (VSP) 271–290
- [27] Kress R 2003 A factorisation method for an inverse Neumann problem for harmonic vector fields *Georgian Math. J.* **10** 549–560

- [28] Lassas M 1997 The impedance imaging problem as a low-frequency limit, *Inverse Problems* **13** 1503–1518
- [29] Monk P 2003 *Finite Element Methods for Maxwell's Equations* (Oxford: Oxford University Press)